International Communications in Heat and Mass Transfer 135 (2022) 106109

Contents lists available at ScienceDirect

International Communications in Heat and Mass Transfer

journal homepage: www.elsevier.com/locate/ichmt

Energy efficient thermal management at low Reynolds number with air-ferrofluid Taylor bubble flows

Madhusree Kole [a,b], Ram Krishna Shah [a], Sameer Khandekar [a,*]

[a] Department of Mechanical Engineering, Indian Institute of Technology Kanpur, UP, India
[b] Department of BS & Hu (Physics), Dr. B.C. Roy Engineering College, Durgapur, WB, India

ARTICLE INFO

Keywords:
Air-ferrofluid Taylor bubble flow
Ferrofluid Convection
Enhanced heat transfer
Low Reynolds number
Numerical simulation

ABSTRACT

Existing thermal management strategies for mini-/micro scale electronic devices have already reached their limits in several applications, necessitating development of innovative heat transfer methods. In this context, a novel heat transfer configuration involving convective heat transfer of two-phase air-ferrofluid Taylor bubble flow in a square mini channel at low Reynolds number (*Re* between 70 and 150) is investigated. Presence of a magnetic field enhances local heat transfer while the pressure drop penalty is not high. Experimental results confirm significant augmentation of heat transfer coefficient, of the order of ~88% to ~95% depending on the flow *Re*. The augmentation strategy is particularly attractive for low *Re* flows, typically encountered in mini-/micro systems, where the induced magnetic forces will be able to dominate the flow inertia. Potential advantages of air-ferrofluid Taylor flows subjected to a magnetic field for heat transfer augmentation is exemplified through this study.

1. Introduction

Micro and mini channels find several applications in heat and mass exchangers, micro-reactors, lab-on-a-chip, micro and nano electro-mechanical systems, fuel cells, biomedical devices, microfluidics, and dissipating heat of power electronics [1]. Improved and more efficient thermal management systems are always in demand for catering to the ever-increasing heat dissipation and enhancing compactness of the devices. The use of single-phase liquid flow in micro/mini channels is one such method. The pioneering experiments with microchannels for dissipating high heat fluxes were done by Tuckerman and Pease in 1981 [2]. In heat exchangers, the use of parallel micro-channels has the potential to dissipate large amount of heat fluxes. However, single-phase liquid flow in miniaturized channels is mostly laminar and thereby has a constant and low *Nu* for fully developed flows. Hence, heat transfer needs to be augmented by utilizing another gas or immiscible liquid as the dispersed phase along with the main continuous liquid phase, i.e., in Taylor bubble flows. Several research groups have established that non-boiling two-phase flows serve as a better solution for dissipating increased heat transfer rates [3–7].

T-junction channels are frequently used to generate Taylor bubble flows. The mechanisms of bubble/droplet formation in T-junction channels depend on the continuous phase *Ca* and are mainly three types viz., squeezing, transitional and dripping. The squeezing flow ($Ca \langle 10^{-2}$) is governed by the squeezing pressure arising due to interfacial tension, dripping flow ($Ca \geq 10^{-2}$) is governed by the shearing stress, and a transitional flow regime exist in between the two, which is governed by a balance between the above two forces [8].The surface tension forces are dominating for the gas-liquid two-phase Taylor bubble flows with $Bo < 4.7$ [9]. A Taylor bubble combined with an adjoining liquid slug is termed as a unit-cell. An elongated gas/vapor bubble separates two adjacent liquid slugs and a thin liquid film usually exists between the gas bubble and channel/tube wall as the gas bubbles travel faster than the liquid [9–12]. The movement of the Taylor bubbles along with the adjacent liquid slugs create substantial disturbance in their 'wake region' due to interfacial interaction, thereby leading to intense mixing or internal recirculation of the liquid molecules and thereby both the heat and mass transport get augmented [13,14].

In general, water is an excellent heat transfer fluid for several applications although it has some restrictions for electronics cooling applications. Previously, a large body of literature on non-boiling two-phase systems, including hydrodynamics and heat transfer, focuses on air-water two-phase flows [15–19]. However, owing to the ever-increasing demands of thermal management in diverse sectors, it will be worth exploring to possibility of enhancing the thermophysical

* Corresponding author.
E-mail address: samkhan@iitk.ac.in (S. Khandekar).

https://doi.org/10.1016/j.icheatmasstransfer.2022.106109

Available online 14 May 2022

Nomenclature

d_h	hydrodynamic diameter of the channel (m)
g	acceleration due to gravity (m/s^2)
h	heat transfer coefficient (W/m^2 K)
q'	input heat flux (W/m^2)
T_W	local heater wall temperature (K)
T_b	estimated local bulk fluid temperature (K)
U_{TP}:	two-phase superficial velocity (m/s) = $U_{SG} + U_{SL}$
U_{SG}	superficial gas-phase velocity (m/s)
U_{SL}	superficial liquid-phase velocity (m/s)

Greek alphabets

λ	Liquid-phase thermal conductivity (W/m K)
β	dynamic hold up of gas-phase
μ_l	dynamic viscosity of the liquid-phase (Pa s)
ρ_l	density of liquid-phase (kg/m^3)
ρ_g	density of gas-phase (kg/m^3)
σ	surface tension of the liquid-phase (N/m)

Non-Dimensional numbers

Bo	Bond number = $\frac{gd_h^2(\rho_l-\rho_g)}{\sigma}$
Ca	Capillary number = $\frac{\mu_l U_{TP}}{\sigma}$
Fr	Froude number = $\frac{U_{TP}}{\sqrt{gd_h}}$
Re_{TP}	two-phase Reynolds number = $\frac{\rho_l U_{TP} d_h}{\mu_l}$
Nu	Nusselt number = $\frac{hd_h}{\lambda}$

properties of water itself and make it more efficient medium. To this effect, ferrofluids, a suspension of superparamagnetic nanoparticles in suitable basefluids like water, ethylene glycol, etc., have gained research attention in the past decade for their enhanced thermophysical properties and heat transfer characteristics when subjected to an external magnetic field [20–24]. Thus, ferrofluids can effectively be used as a heat removing agent in a two-phase flow configuration without involving phase change.

Very few studies exist in the open literature on ferrofluids acting as one of the phases of two-phase Taylor flows in micro/mini channels [8,25–28]. One representative study on heat transfer of ferrofluids acting as the dispersed phase of two-phase liquid-liquid Taylor flow in micro/mini channels is reported by Gui et al. [26]. In this context, the present study involves a novel experimental and numerical simulation work on the convective heat transfer of air-ferrofluid Taylor bubble train flow, under the action of a magnetic field. The transport phenomena of Taylor bubbles/slug flows are complex in nature and their thermo-hydrodynamics depend on several parameters such as slug and bubble lengths (phase distribution or flow morphology), liquid film thickness, gas fraction/dynamic hold up of gas phase, bubble velocity, Reynolds (*Re*) and Capillary number (*Ca*) of the flow [29–31]. Our present investigation demonstrates that the transport characteristics of the non-boiling Taylor bubble/slug flow can be augmented by altering the flow morphology through external magnetic field, even though the geometrical and flow parameters are kept identical. In earlier studies, the two-phase flow morphology was varied either by changing the geometrical configuration with different sizes of T-junctions [29,32] or the flow parameters [16,17,19]. In all such cases, flow morphology was not identical when heat transfer rate was compared. It is also well established that higher gas fraction deteriorates the heat transfer augmentation [26,29,32]. However, with the application of magnetic field we obtained an increased heat transfer even at higher gas fractions.

2. Experiments

Magnetite (Fe_3O_4) nanoparticles are first chemically synthesized by the co-precipitation method and then coated with lauric acid before dispersing in distilled water [8]. The experimentally measured values of thermal conductivity, viscosity, surface tension, and saturation magnetization of the prepared ferrofluids are given in Table 1. The details of the equipment for measuring the physical properties of the samples are given in [8].

A square channel of cross-section size 3.0 mm × 3.0 mm with a T-junction assembly is fabricated from a 12 mm thick polymethylmethacrylate (PMMA) sheet. The schematic of the experimental set-up is shown in Fig. 1 (a). The cross-sectional side view of the channel is shown Fig. 1 (b). A thin (70 μm) stainless-steel strip heater of length 150 mm is attached such that it acts as one of the walls of the channel. We turn and orient the whole set-up in a preferred way so that the thin foil heater itself becomes either the bottom or top wall of the channel. This type of set up, with a strip heater forming one wall of the channel is very appropriate for mimicking heat dissipation configurations in the electronics industry where one can mount the hot micro-chip in place of the strip heater. The time taken for heat to diffuse across the heater wall is ~1.46×10^{-3} s. Therefore, the temperatures at both sides of the heater wall (i.e., PMMA and channel sides) can be treated as nearly identical. A DC power supply (V: 0–60 V and I: 0–50 A) is used for heating such that a constant heat flux thermal boundary condition is maintained. Experiments are done at three different input heat fluxes viz.: ~7267, ~9779, and ~ 13,441 W/m^2 for the air-ferrofluids two-phase flow. Five K-type thermocouples (M/S Omega, bead diameter 0.5 mm) are fixed at the heater wall at 25 mm distance apart along the PMMA wall side. One more thermocouple is inserted within the channel in the downstream direction to measure the bulk fluid outlet temperature.

Magnetite-water ferrofluids (nanoparticles concentrations of 0.25 vol%, 0.5 vol% and 1 vol%) and air are pumped at two ends of the T-junction using syringe pump #1 (M/S. Cole-Parmer, model WW-74900) and syringe pump #2 (M/S. New Era Pump Systems, Inc., model NE 4000), respectively as shown in Fig. 1 (a). Two different permanent magnets (Magnet #1 and Magnet #2) are used to study the effect of magnetic field. The value of magnetic field is measured by placing the magnets at different distances from the probe/sensor using a Gaussmeter (M/s F.W. BELL, model 6010) as shown in Fig. 1 (c).

During the experiments, the bubble length and generation frequency are measured from the digitally acquired images using a DSLR camera (model: Nikon 7100) with micro-lenses (model: Nikkor 85 and 200 mm). The images have a resolution of 25 μm/pixel. The local Heat Transfer Coefficient (HTC), h and corresponding Nu estimated at five different thermocouple locations in the downstream direction are given as: $h = q'/(T_W - T_b)$ and $Nu = hd_h/\lambda$, respectively. The two-phase Reynolds number is given as: $Re_{TP} = \rho_l U_{TP} d_h/\mu_l$. The local bulk fluid temperatures along the channel are estimated from the linear interpolation of the measured inlet and outlet temperatures of the fluid. The dynamic holdup of gas-phase in the channel is given as: $\beta = \frac{U_{SG}}{U_{SL}+U_{SG}}$. The uncertainty in measurement of HTC is given as: $\frac{\Delta h}{h} = \sqrt{\left(\frac{\Delta V}{V}\right)^2 + \left(\frac{\Delta I}{I}\right)^2 + \left(\frac{\Delta l}{l}\right)^2 + \left(\frac{\Delta w}{w}\right)^2 + 2\left(\frac{\Delta T}{T}\right)^2}$, where V, I, l and w are the input voltage, current, length and width of the heater, respectively. It is estimated to be within ~7%. The uncertainty of all measured/calculated parameters is given in the appendix section (Table A1).

3. Results and discussions

3.1. Experimental

The experimental setup is benchmarked at first with the single-phase water flow data compared with the correlation given by Muzychka and Yovanovich [33] as shown in Fig. 2 (a). The correlation [33] is given as:

Table 1
Thermophysical and magnetic properties of the prepared ferrofluids at 25°C.

Conc. of Fe_3O_4 nanoparticles	Density (kg/m^3)	Saturation magnetization (A/m)	Thermal conductivity (W/m K)	Viscosity (Pa s) $\times 10^{-4}$	Surface tension (N/m) $\times 10^{-3}$
0 vol% (Water with lauric acid)	995 ± 2	NA	0.60 ± 0.01	8.9 ± 0.2	34 ± 1.4
0.25 vol%	1004 ± 3	697 ± 18	0.62 ± 0.01	9.3 ± 0.2	28 ± 1.3
0.5 vol%	1015 ± 4	1461 ± 37	0.64 ± 0.01	9.5 ± 0.2	26 ± 1.3
1 vol%	1032 ± 6	2972 ± 75	0.72 ± 0.02	10 ± 0.3	20 ± 1.3

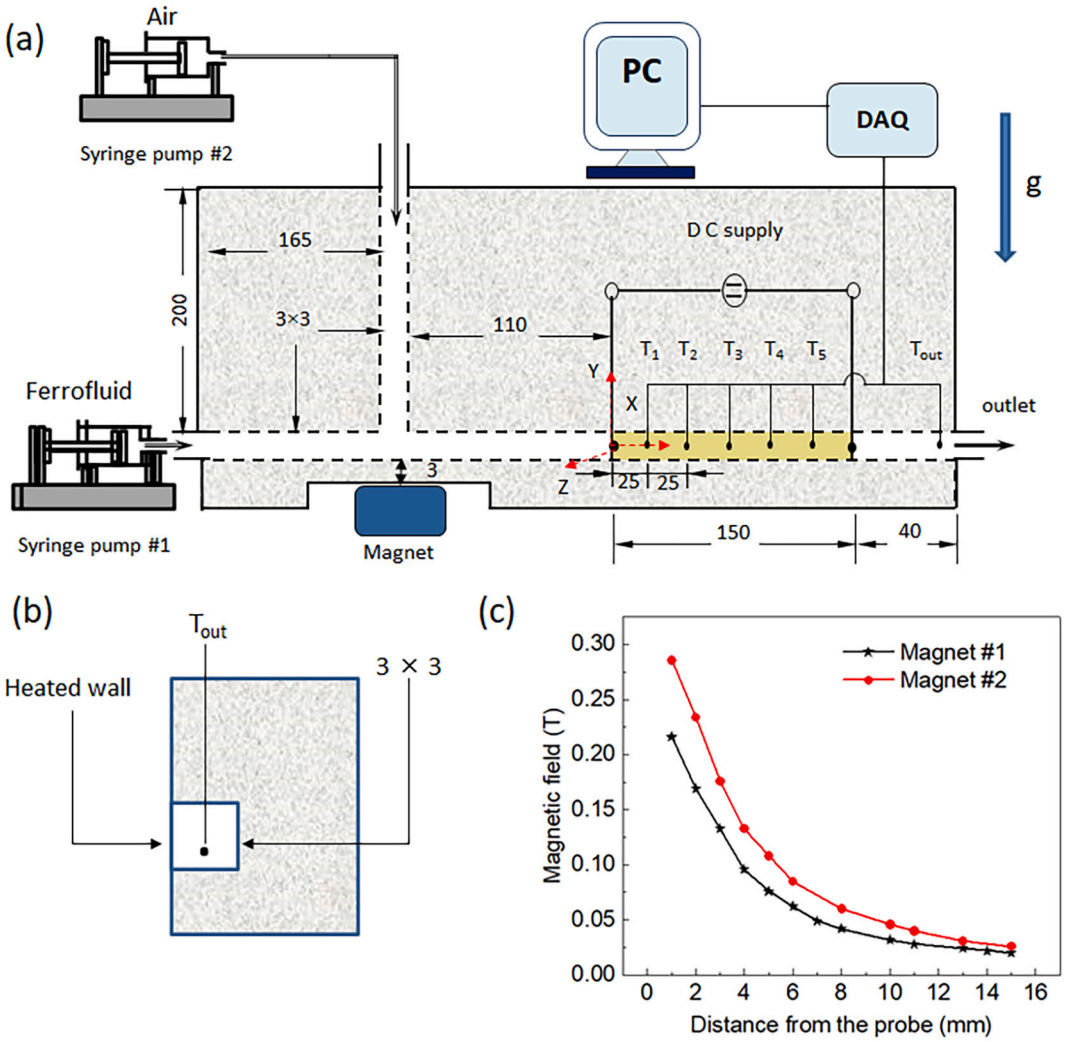

Fig. 1. (a) Schematic of the experimental set-up. (b) Cross-sectional side view of the channel. All dimensions are in mm. (c) Magnetic field as a function of distance from the probe of the Gaussmeter. Lines serve as guide to the eye.

$$Nu_{Local} = \left[\left(1.302/x^{*(1/3)}\right)^5 + 3.61^5\right]^{(1/5)} \quad (1)$$

where, non-dimensional length $x^* = x/\ Re\ .\ Pr\ .\ d_h$, x is the local thermocouple position from starting point of the heater, and Pr is the Prandtl number of the fluid.

Then, keeping the air flow rate constant at 10 ml/min (superficial velocity = 0.0185 m/s), water flow rate is increased from 2.5 ml/min to 15 ml/min in steps of 2.5 ml/min. The average HTC increases with the Re_{TP}. The increase in average Nu ($\overline{Nu}$) with Re_{TP} for air-water two-phase flow is explained well with the correlations given by Walsh et al. [34] and Leung et al. [32] as shown in inset of Fig. 2 (a). The equation by Walsh et al. [34] is given as:

$$\overline{Nu} = (1-\beta)\left[3.61 + 25(L_{LS}/d_h)^{-0.5}\right] \quad (2)$$

where, L_{LS}: length of the liquid slug, and the correlation developed by Leung et al. [32] is given as:

$$\overline{Nu} = (1-\beta)\left[3.61 + \frac{0.29}{\left(L_{LS}^* + 0.15{L_{LS}^*}^{0.33}\right)}\right] \quad (3)$$

where, $L_{LS}{}^* = L_{LS}/Re_{TP}.\ Pr\ .\ d_h$.

It may be noted that the bottom wall heater configuration provides more heat transfer augmentation compared to the top wall. The gravitational force may become important for gas-liquid flow in millimeter-size channels, as the Froude number for a 1 mm channel are calculated to be 0.01, 1 and 100 for superficial velocities of 0.01, 0.1 and 1 m/

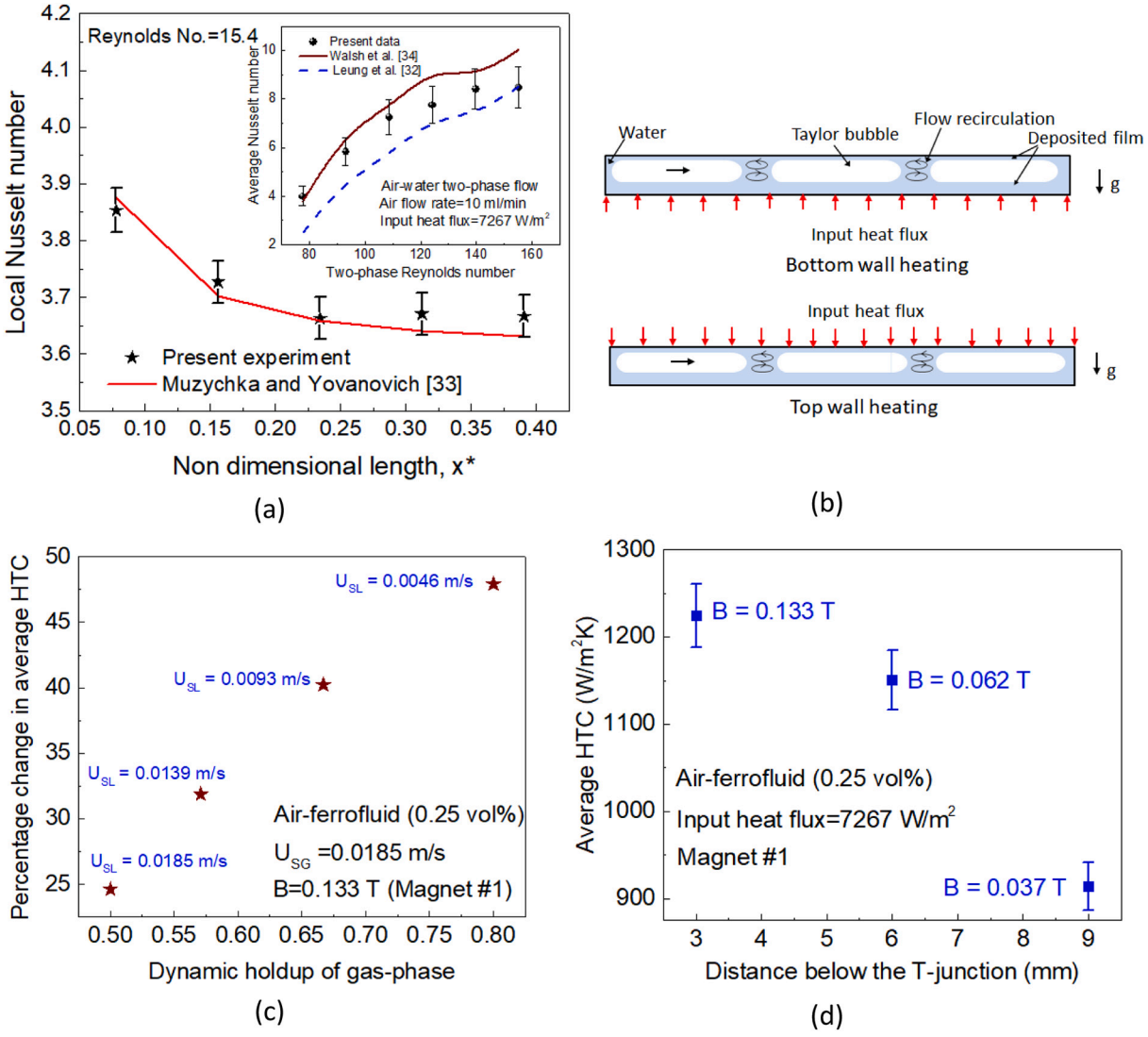

Fig. 2. (a) Experimental data and correlation [33] for single-phase water flow. Inset shows $\overline{Nu}$ vs. two-phase Reynolds number of air-water for the bottom wall heating, and compared with eqs. (2) [34] and (3) [32], respectively. (b) Schematic representation of the deposited thin film and flow recirculation occurring for bottom and top wall heating for air-water case. (c) Percentage enhancement in average HTC of air-ferrofluid (0.25 vol%) compared to no-magnet case as a function of β at magnetic field 0.133 T for bottom wall heating. (d) Average HTC vs. distance of Magnet #1 below the T-junction for air-ferrofluid (0.25 vol%).

s, respectively [9]. So, the Taylor bubbles move slightly upwards due to the buoyancy effect as shown in Fig. 2 (b). For the bottom wall heating, a greater number of liquid-phase molecules take part in the heat transfer process in comparison to the top wall configuration. The heat transfer capacity of the liquid is greater than that of the gas, so more heat transfer is obtained for the bottom wall heater configuration. Thus, we have opted for the bottom wall heating for all experiments with air and ferrofluids.

Subsequently, while performing preliminary two-phase experiments with air and ferrofluid (0.25 vol%) at an input heat flux of ~7267 W/m^2, we have observed that by placing Magnet #1 (B = ~0.133 T) at 3 mm below the T-junction, maximum enhancement in average HTC with respect to no-magnet case, occurs when β is 0.8 as shown in Fig. 2 (c). The average HTC enhances by ~48% at ferrofluid and air flow rate of 2.5 ml/min and 10 ml/min, respectively i.e., at Re_{TP} = 74.8 in comparison to no-magnet case (B = 0). This increment decreases and becomes only 25% when the Re_{TP} increases to 119.8 (β = 0.5). Thus, it is seen that magnetic forces become important and dominate over inertial forces at low flow rates of the ferrofluid, leading to heat transfer intensification. With increase in ferrofluid flow rate, the effect of inertial forces overtakes the magnetic forces, and the resultant heat transfer augmentation rate deteriorates. It is also observed that maximum heat transfer augmentation occurs when the magnet is placed 3 mm below the T-junction as shown in Fig. 2 (d). As distance of the magnet below the T-junction increases, the magnetic field decreases which is in line with Fig. 1 (c). Thus, for all further experiments, we have kept β as 0.8, and placed both the magnets at 3 mm below the T-junction. The air flow rates are chosen to be 10, 12, 16, and 20 ml/min; and the ferrofluids flow rates as 2.5, 3, 4, and 5 ml/min, respectively.

The Capillary number for the present air-ferrofluid flow lies within ~0.7–2.31 × 10^{-3}. So, for no-magnet case, bubbles are formed due to the squeezing pressure produced by the growing air bubble at the T-junction. In absence of magnetic field, the average HTC of air-ferrofluid two-phase does not enhance much at low flow rates of air (10 ml/min) and water/ferrofluid (2.5 ml/min) as shown in Fig. 3 (a). The average HTC increases by only ~16%, for air-ferrofluid (1 vol%) compared to air-water case. The corresponding Re_{TP} of air-water and air-ferrofluid (1 vol%) being 77.6 and 71.5, respectively. In presence of the magnets, it is observed that local heater wall temperature decreases, and the bulk fluid temperature increases. Thus, local intra-phase mixing enhances, augmenting the heat transfer. With application of magnetic field (Magnet #2, ~0.177 T), the average HTC of air-ferrofluid (1 vol%) enhances

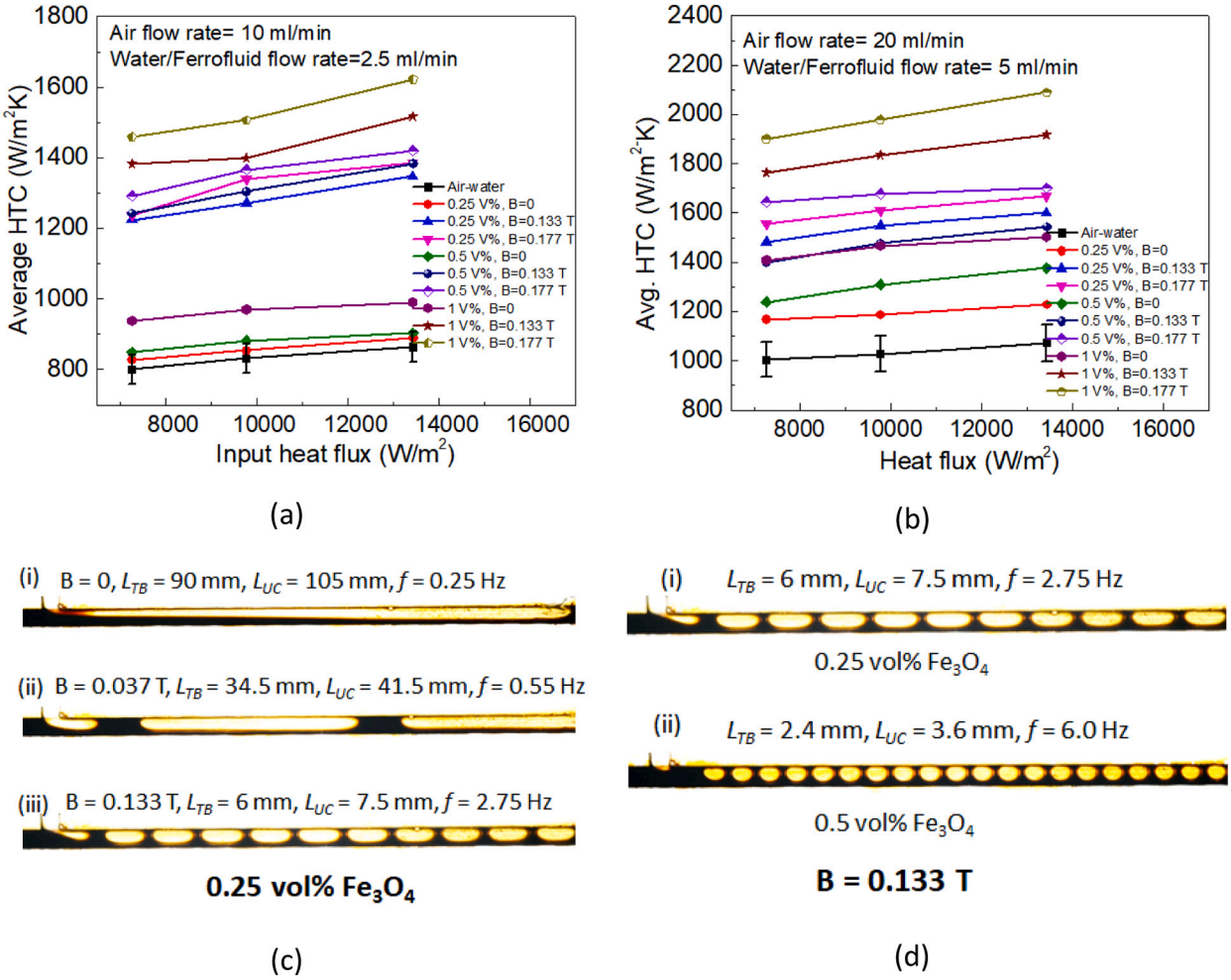

Fig. 3. Average HTC vs. input flux of air-water and different air-ferrofluids at (a) air and water/ferrofluids flow rate of 10 ml/min and 2.5 ml/min, respectively. (b) air flow rate of 20 ml/min and water/ferrofluids flow rate of 5 ml/min, respectively. Lines in (a) and (b) serve as guide to the eye. The images showing effect of (c) external magnetic field, and (d) concentration of Fe_3O_4 nanoparticles in the ferrofluids, on the hump formation and splitting of bubbles while crossing the hump. Air and ferrofluid flow rates are 10 and 2.5 ml/min, respectively in both (c) and (d).

significantly by ~88% compared to air-water, at an input heat flux of ~13,441 W/m^2. The same heat transfer rate can be attained by air-water flow with four times (10 ml/min) higher water flow rate. The two-phase pressure drop developed per unit length of the channel is calculated from the following equation as given by Kreutzer et al. [35]:

$$\frac{\Delta p}{L} = (1-\beta)\frac{4}{d_h}\left(\frac{1}{2}\rho_l U_{TP}^2\right)\frac{16}{Re_{TP}}\left[1 + a\frac{d_h}{L_{LS}}\left(\frac{Re_{TP}}{Ca}\right)^{0.33}\right] \quad (4)$$

where, a is a constant (~0.07–0.17). Here obtained values for the pressure drop per unit length for air-water and air-ferrofluid (1 vol%) are 58.65 and 16.56 Pa/m at Re_{TP} of 124.16 and 71.5, respectively. Hence, the required pumping power to achieve similar HTC is substantially reduced with ferrofluids.

When air flow rate is increased to 20 ml/min (superficial velocity = 0.037 m/s) and water/ferrofluid (1 vol%) flow rate to 5 ml/min (superficial velocity = 0.0093 m/s), respectively, the average HTC increases by ~40% compared to air-water for no-magnet case. The corresponding Re_{TP} of air-water and air-ferrofluid (1 vol%) being 155.3 and 143.3, respectively. Under the action of Magnet #1 (0.133 T) and Magnet #2 (0.177 T), the average HTC enhances by ~79% and ~ 95%, respectively as shown in Fig. 3 (b). $\overline{Nu}$ increases from 5.36 for air-water to 7.99 and 8.7 for air-ferrofluid (1 vol%) when subjected to Magnet #1 (~0.133 T) and Magnet #2 (~0.177 T), respectively at an input heat flux of ~13,441 W/m^2.

It is observed that both length of the Taylor bubble (L_{TB}) and unit-cell (L_{UC}) decrease with increasing magnetic field (Fig. 3 (c)) and also with increase in Fe_3O_4 nanoparticles concentration in the ferrofluids (Fig. 3 (d)). An attractive magnetic force is induced in the superparamagnetic nanoparticles in ferrofluids by the permanent magnets placed below the T-junction. The intensity of this induced magnetic force depends both on the gradient of the magnetic field and the magnetization of ferrofluid [8]. As a result, a hump-shaped ferrofluid flocculate is formed at the T-junction. The flow passage area is constricted, and a local magnetic pressure barrier is created at the interface, which alters the hydrodynamics of the two-phase flow [8]. This results in the early necking and pinching off the bubbles. Hence, bigger bubbles split into smaller ones and bubble generation frequency (f) increases compared to the no-magnet case. Thus, the flow field gets disturbed by giving rise to secondary flow in liquid slugs enhancing the transport of momentum and energy in turn.

3.2. Numerical simulation

A phase-field based numerical investigation is carried out on the incompressible, non-boiling, and immiscible two-phase flow in two-dimensional (2D) planer configuration using COMSOL® Multiphysics software. The numerical modelling involves modelling multi-physics

phenomena involving coupling of magnetic field, fluid flow and heat transfer and multiphase flow (capturing evolution of interfaces and topological changes). Ferrofluid is assumed to be pseudo single-phase liquid in the modelling. The Taylor bubble flow of air-ferrofluid (0.5 vol%) is modelled in T-junction channels in terms of the fixed frame of reference approach, both in absence and presence of an externally applied magnetic field below the T-junction. A schematic of the geometry is shown in Fig. 4 (a). Here, the channel width is taken to be 3 mm. A 2D spatially distributed magnetic field is simulated using a line dipole of strength, *m*. A small section (30 mm) of the main fluidic channel is heated by uniform heat flux (q' = 20 kW/m^2) applied on both top and bottom wall boundary conditions, as illustrated in Fig. 5 (a). The inflow temperature is taken as 293.15 K. The energy balance equation is solved along with the continuity, momentum, Cahn-Hilliard phase-field [36,37], and Maxwell equations. The numerical simulation methodology adopted in this study is elaborated in the appendix section.

The length and bubble formation frequency of the Taylor bubbles for no-magnet case are shown in Fig. 4 (a). The effect of applied magnetic field strength on L_{TB}, L_{UC}, and f is shown in Fig. 4 (b). It is found that both the Taylor bubble and slug lengths get reduced by ~70% at an applied magnetic field strength of 0.8 A m^2, compared to no-magnet case. A large increase in local fluid pressure is clearly observed (Fig. 4 (b)) at the vicinity of the magnet i.e., at the T-junction. The local bubble pressure varies due to curvature effect and the fluid starts flowing from a narrow passage area at higher local shear velocity. This results in reduction in bubble size and increase in its generation frequency. The ratio of length of the Taylor bubble and unit cell with the ratio of ferrofluid superficial velocity and sum of air and ferrofluid superficial velocities as obtained from the present numerical simulation for no-magnet case is validated with the correlation given by Thulasidas et al. [38]: $L_{TB}/L_{UC} = 1 - U_{SL}/U_{TP}$ and our results are in very well agreement within 3%. The corresponding ratio of L_{TB}/L_{UC} and U_{SL}/U_{TP} in the present case is 11.7/19.5 = 0.6 and 0.03/0.07 = 0.43, respectively.

The effect of changes in flow morphology on the temperature field can be seen in Figs. 5 (a) and (b) for uniform heat flux boundary conditions. The maximum temperature for bigger bubbles reaches 312 K while it is at 306 K for smaller bubble (m = 0.8 A m^2) cases. The axial variations of time-averaged wall temperature and local *Nu* for uniform heat flux case are presented in Figs. 5(c) and (d), respectively. It is found that wall temperature reduces and *Nu* enhances in presence of the magnet. Thus, generation of smaller bubbles/unit-cells through external magnetic manipulation is effective in enhancing heat transfer which matches with the experimental findings of us. Researchers [5–7,26] also confirmed that shorter plugs enhance heat transfer.

4. Conclusions

Convective heat transfer of air-ferrofluid two-phase Taylor bubble train flow in a mini channel with T-junction is experimentally investigated for the first time. Air and Fe_3O_4-water ferrofluids are flown at calculated velocities such that the dynamic holdup of gas-phase remains 0.8 and the two-phase Reynolds number varies from ~70–150. Effect of magnetic field is studied by placing two permanent magnets 3 mm below the T-junction. Numerical simulation is also carried out to evaluate the heat transfer of air-ferrofluid two-phase flow. Both experimental and numerical results confirm the splitting of larger bubbles into smaller ones with higher frequency in presence of the magnets. This results in the heat transfer intensification.

The bottom wall heater configuration is tested to be more efficient compared to the top wall. With decreasing value of β or increasing value of Re_{TP}, inertial forces become predominant over the magnetic forces. The experimental results show substantial enhancement of convective HTC in presence of a magnet at low Reynolds number. Maximum augmentation achieved is ~95% with air-ferrofluid (1 vol%) at Re_{TP} = 143.3 in presence of Magnet #2 (0.177 T). The pressure drop developed per unit length of the channel and hence required pumping power to

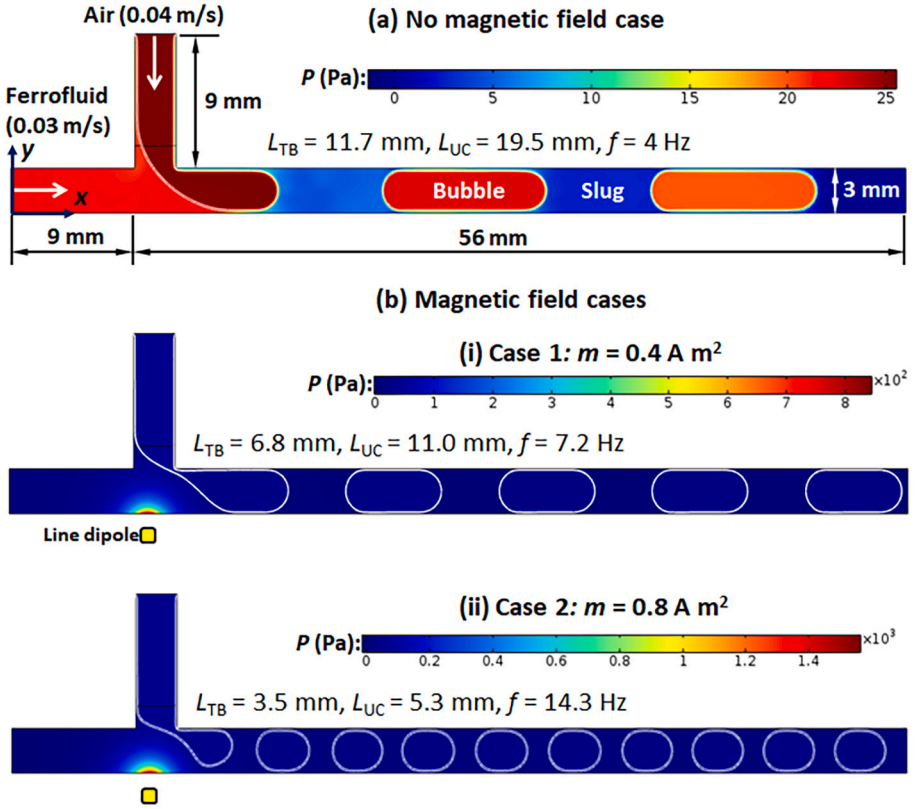

Fig. 4. (a) Unit-cell size and bubble generation frequency at no-magnet case, (b) Effect of magnetic field on L_{TB}, L_{UC}, and f at (i) m = 0.4 A m^2 (ii) m = 0.8 A m^2.

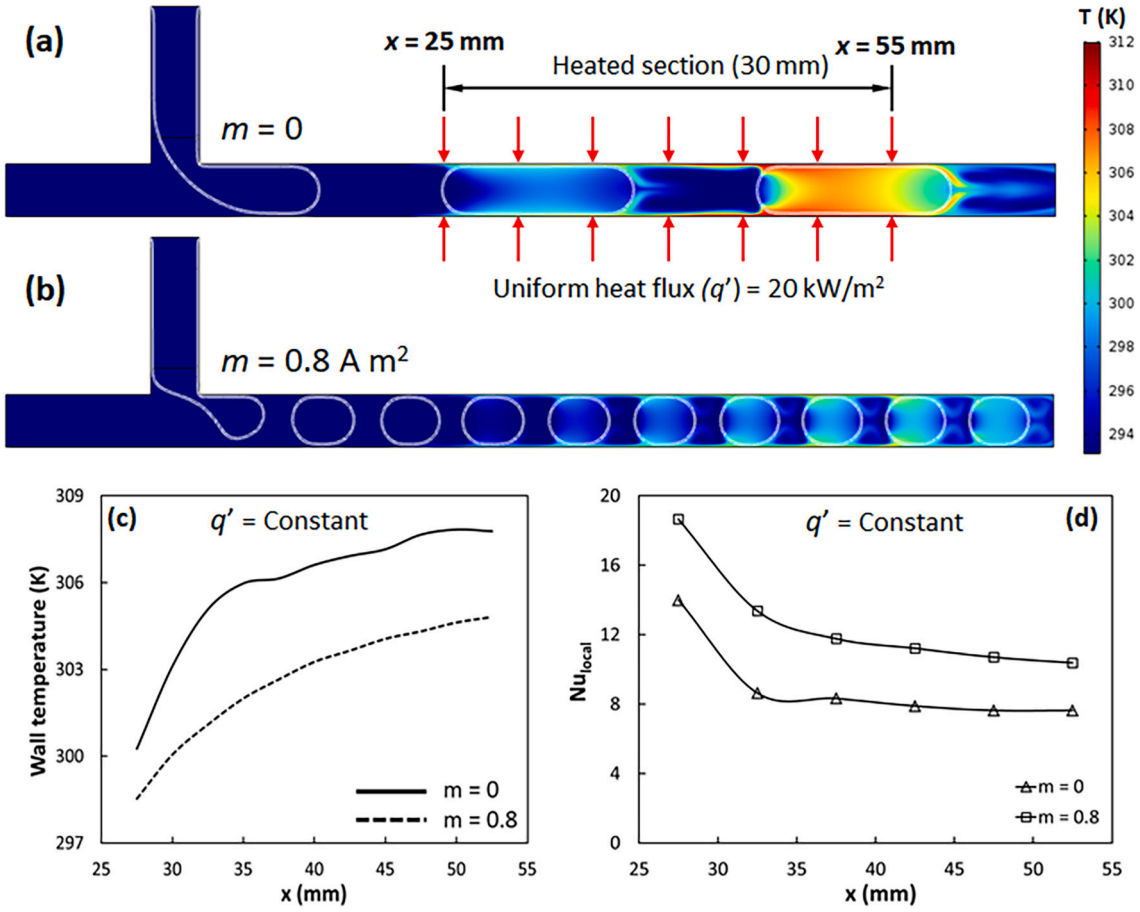

Fig. 5. (a) Temperature distribution in constant heat flux cases for $m = 0$ and (b) $m = 0.8$ A m^2. (c) Time-averaged axial variation of wall temperature. (d) Local ***Nu*** vs. axial location.

achieve the same HTC is reduced with ferrofluids, rendering them as potential energy efficient thermal management candidates.

Author contributions

Sameer Khandekar conceived and supervised the project.

Both, Madhusree Kole and Ram Krishna Shah designed the experiments.

Madhusree Kole performed the experiments and wrote the manuscript. Ram Krishna Shah did the numerical simulations.

All authors edited the manuscript and figures and approved the final version for submission.

Declaration of Competing Interest

The authors declare that they have no known competing financial interests or personal relationships that could have appeared to influence the work reported in this paper.

Acknowledgement

The authors would like to thank IIT Kanpur for providing the necessary facilities to conduct this work.

Appendix

A1 Uncertainty analysis

The uncertainty in flow rate/superficial velocity comes from the accuracy in the dispensing of syringe pumps. For the measurement of Taylor bubble/unit-cell lengths, uncertainty comes from defining pixel resolution of the known distance and the measurement of unit-cell length in pixels from the acquired images. Heat flux is calculated from the input heat and the length and width of the heater element. The estimated maximum possible uncertainties in the measured/calculated quantities are given in Table A1.

Table A1
Maximum uncertainty in the measured/calculated variables.

Sl. no.	Parameter	Range	Maximum uncertainty
1.	Flow rate (Q)	2.5–30 ml/min	±1.0%

(*continued on next page*)

Table A1 (*continued*)

Sl. no.	Parameter	Range	Maximum uncertainty
2.	Temperature (T)	20–60°C	±0.5%
3.	Voltage (V)	0–60 V	±0.5%
4.	Current (I)	0–50 A	±0.5%
5.	Image resolution	25 μm/pixel	±3.0%
6.	L_{TB}, L_{UC}	2–110 mm	±7.5%
7.	Heat flux (q')	7–14 kW/m^2	±6.0%
8.	Heat transfer coefficient (h)	500–2200 (W/m^{2}K)	±6.5%
9.	Nusselt number (Nu)	2–10	±7.0%

A2 Methodology for Numerical Simulation

A single set of continuity, momentum and energy equations is solved to simulate the thermo-hydrodynamics of the Taylor bubble flow (TBF) of air and ferrofluid. Flow is assumed to be incompressible, immiscible, and non-boiling. Ferrofluid (ff) is modelled as pseudo single-phase liquid. Surface tension (f_{ST}) and magnetic (f_k) forces are added as body force terms in the momentum equation. The evolution of the interface and formation of bubbles is implicitly captured using the Cahn-Hilliard phase-field (CH PF) equation [36,37,39]. The PF method is a diffuse interface method based on the free energy of the system. In PF formulation, phases are distinguished using a scaler ordered parameter called phase-field parameter (ϕ). It is assigned distinctive values for the bulk phases (e.g., −1 and + 1 for air and ferrofluid in the present case), and the interfacial region is represented by a rapid but smooth transition of ϕ.

Following partial differential equations (PDEs) are solved to simulate the thermo-hydrodynamics of the TBF of air and ferrofluid in the domain of interest:

$$\nabla .u = 0 \tag{A-1}$$

$$\rho_{mix}\frac{\partial u}{\partial t} + \rho_{mix}(u.\nabla)u = -\nabla P + \mu_{mix}\nabla^2 u + f_k + f_{ST} \tag{A-2}$$

$$\frac{\partial T}{\partial t} + u.\nabla T = \left(\frac{k_{mix}}{\rho_{mix}C_{p_{mix}}}\right)\nabla^2 T \tag{A-3}$$

$$\frac{\partial \phi}{\partial t} + u\bullet\nabla\phi = \nabla\bullet\gamma\nabla \mathrm{G}$$

$$G = \lambda\left[-\nabla^2\phi + \frac{\phi\left(\phi^2 - 1\right)}{\varepsilon^2}\right] \tag{A-4}$$

$$\nabla .B = 0; B = \mu_0(H + M) \tag{A-5}$$

where, u, P and T represent velocity, pressure, and temperature, respectively. G is a thermodynamic property called the chemical potential of the fluid system. λ, γ, and ε are PF model parameters called mixing energy density (N), mobility (m^3 s/kg), and interfacial thickness parameters, respectively. Surface tension (σ), λ, γ, and ε are related as follows:

$$\sigma = \frac{2\sqrt{2}}{3}\frac{\lambda}{\varepsilon}; \gamma \sim \varepsilon^2 \tag{A-6}$$

Surface tension and magnetic forces are defined as follows:

$$f_{ST} = G\nabla\phi; f_k = \mu_o(M.\nabla)H \tag{A-7}$$

where, M and H are magnetization and magnetic field, respectively. Magnetization of 0.5 vol% ferrofluid sample is measured using a vibration sample magnetometer and given as an input parameter in the simulation. Applied 2D magnetic field of a line dipole is simulated using Gauss divergence law with the following Eq. [21]:

$$V_m = \frac{m\,sin\theta}{r}; H = -\nabla V_m; H = \frac{m}{r^2}(sin\theta\hat{r} - cos\theta\hat{\theta});$$

$$r = \sqrt{(x - X)^2 - (y - Y)^2}; \theta = tan^{-1}\left(\frac{y - Y}{x - X}\right) \tag{A-8}$$

where, V_m is the magnetic scalar potential of the line dipole. X and Y are the coordinate location of the dipole as per the Cartesian coordinate (x, y) system. r and θ are the polar coordinates defined in terms of x and y, and m is the strength of the magnetic dipole, which is varied to change the intensity of the applied field.

Thermophysical properties of the mixture are defined in terms of properties of two phases and their volume fractions as follows:

$$\rho_{mix} = \rho_{air}Vf_{\mathrm{air}} + \rho_{ff}Vf_{ff}$$

$$\mu_{mix} = \mu_{air}Vf_{air} + \mu_{ff}Vf_{ff}$$

$$k_{mix} = k_{air} Vf_{air} + k_{ff} Vf_{ff}$$

$$C_{p\,mix} = C_{p\,air} Vf_{air} + C_{p\,ff} Vf_{ff} \tag{A-9}$$

The volume fraction of two phases is computed in terms of ϕ as follows:

$$Vf_{air} = \frac{1-\phi}{2}; Vf_{ff} = \frac{1+\phi}{2} \tag{A-10}$$

Considering both density and heat capacity as dependent of space and time, the bulk fluid temperature (T_b) is defined in the following way [40]:

$$T_b = \frac{\int_0^R \rho(r) C_p(r) u(r) T(r) dr}{\int_0^R \rho(r) C_p(r) u(r) dr} \tag{A-11}$$

The governing equations are subjected to certain boundary conditions (BCs). Continuity and momentum equations are subjected to no-slip ($u = 0$) BC on the walls, and fluid velocities are defined at the two inlets. At outlet, zero-gauge pressure ($P = 0$) is defined. For the energy equation, the inlet temperature of fluids is defined ($T_{\text{in}} = 293.15$ K) at the two fluid inlets, and an outflow condition is defined at the outlet. Thermal insulation ($n.q' = 0$) BC is defined on the walls except for the heated section where uniform heat flux ($q' = 20$ kW/m^2) is defined. ϕ is assigned -1 and $+1$ for air and ferrofluid domains, and wetting boundary condition is defined on the walls as follows:

$$n.G = 0; n.\nabla\phi = cos\,(\theta_w)\,|\nabla\phi| \tag{A-12}$$

where, n and θ_w are normal to the surface and wall contact angle, respectively.

The governing PDEs of mass, momentum and energy balance, Maxwell equation for the magnetic field and the PDE of CH PF model (Eqs. (A-1) - (A-5)) with boundary conditions specified above are solved on COMSOL® Multiphysics platform. A default fully coupled approach with PARDISO linear solver is used for the solution of coupled PDEs. Time integration is done through implicit variable order backward differentiation formula (BDF) with free time stepping. The spatial discretization is performed using triangular mesh elements of the following orders: first-order elements are set for velocity, pressure, temperature and PF parameter variables and second-order elements are used for magnetic field equation. Mesh element size (h) of 0.03 mm (1% of the channel width) is used to discretize the computational domain. Mesh size is selected based on the recommendations of earlier works on PF based modelling, which suggested the mesh size less than 2% of the characteristic length (width in the present case) is required for accurate resolution of the interfacial stresses [39,41]. Interfacial thickness parameter is kept equal to the mesh element size (h) in simulations.

References

[1] T. Bandara, N.-T. Nguyen, G. Rosengarten, Slug flow heat transfer without phase change in microchannels: a review, Chem. Eng. Sci. 126 (2015) 283–295.
[2] D.B. Tuckerman, R.F.W. Pease, High-performance heat sinking for VLSI, IEEE Electron Device Letters 2 (5) (1981) 126–129.
[3] A.R. Betz, D. Attinger, Can segmented flow enhance heat transfer in microchannel heat sinks? Int. J. Heat Mass Transf. 53 (19–20) (2010) 3683–3691.
[4] Z. Che, T.N. Wong, N.-T. Nguyen, Heat transfer in plug flow in cylindrical microcapillaries with constant surface heat flux, Int. J. Therm. Sci. 64 (2013) 204–212.
[5] J. Liu, et al., Numerical and experimental investigations of the formation process of ferrofluid droplets, Microfluid. Nanofluid. 11 (2) (2011) 177–187.
[6] Z. Che, T.N. Wong, N.-T. Nguyen, Heat transfer enhancement by recirculating flow within liquid plugs in microchannels, Int. J. Heat Mass Transf. 55 (7–8) (2012) 1947–1956.
[7] P.T. Bandara, Heat Transfer Enhancement in Microchannels with Liquid-Liquid Slug Flow, RMIT University, 2015.
[8] R.K. Shah, S. Khandekar, Manipulation of Taylor bubble flow in a magneto-fluidic system, Colloids Surf. A Physicochem. Eng. Asp. 593 (2020), 124589.
[9] R. Gupta, D. Fletcher, B. Haynes, Taylor flow in microchannels: a review of experimental and computational work, The J. Computat. Multiphase Flows 2 (1) (2010) 1–31.
[10] S. Haase, Characterisation of gas-liquid two-phase flow in minichannels with co-flowing fluid injection inside the channel, part I: unified mapping of flow regimes, Int. J. Multiphase Flow 87 (2016) 197–211.
[11] S. Haase, Characterisation of gas-liquid two-phase flow in minichannels with co-flowing fluid injection inside the channel, part II: gas bubble and liquid slug lengths, film thickness, and void fraction within Taylor flow, Int. J. Multiphase Flow 88 (2017) 251–269.
[12] T. Abadie, et al., Hydrodynamics of gas–liquid Taylor flow in rectangular microchannels, Microfluid. Nanofluid. 12 (1) (2012) 355–369.
[13] V. Srinivasan, et al., Oscillation of an isolated liquid plug inside a dry capillary, Heat Mass Transf. 53 (11) (2017) 3353–3362.
[14] H. Kinoshita, et al., Three-dimensional measurement and visualization of internal flow of a moving droplet using confocal micro-PIV, Lab Chip 7 (3) (2007) 338–346.
[15] A. Majumder, B. Mehta, S. Khandekar, Local Nusselt number enhancement during gas–liquid Taylor bubble flow in a square mini-channel: an experimental study, Int. J. Therm. Sci. 66 (2013) 8–18.
[16] B. Mehta, S. Khandekar, Measurement of local heat transfer coefficient during gas–liquid Taylor bubble train flow by infra-red thermography, Int. J. Heat Fluid Flow 45 (2014) 41–52.
[17] B. Mehta, S. Khandekar, Taylor bubble-train flows and heat transfer in the context of pulsating heat pipes, Int. J. Heat Mass Transf. 79 (2014) 279–290.
[18] H.B. Mehta, J. Banerjee, Experimental investigations on thermo-hydrodynamics of continuous Taylor bubble flow through minichannel, Int. J. Heat Mass Transf. 94 (2016) 119–137.
[19] H.B. Mehta, J. Banerjee, An investigation of flow orientation on air–water two-phase flow in circular minichannel, Heat Mass Transf. 50 (10) (2014) 1353–1364.
[20] J. Singh Mehta, et al., Convective heat transfer enhancement using ferrofluid: a review, J. Thermal Sci. Eng. Applicat. 10 (2) (2018).
[21] R.K. Shah, S. Khandekar, Exploring ferrofluids for heat transfer augmentation, J. Magn. Magn. Mater. 475 (2019) 389–400.
[22] M.H. Buschmann, Critical review of heat transfer experiments in ferrohydrodynamic pipe flow utilising ferronanofluids, Int. J. Therm. Sci. 157 (2020), 106426.
[23] M. Kole, S. Khandekar, Engineering applications of ferrofluids: a review, J. Magn. Magn. Mater. 537 (2021), 168222.
[24] N.G.J. Gui, et al., Ferrofluids for heat transfer enhancement under an external magnetic field, Int. J. Heat Mass Transf. 123 (2018) 110–121.
[25] Q. Zhang, et al., Micro-magnetofluidics of ferrofluid droplet formation in a T-junction, Colloids Surf. A Physicochem. Eng. Asp. 537 (2018) 572–579.
[26] N.G.J. Gui, et al., Ferrofluidic plug flow heat transfer enhancement, Int. J. Computat. Methods Exp. Measur. 6 (2) (2018) 291–302.
[27] J. Liu, Y.F. Yap, N.-T. Nguyen, Numerical study of the formation process of ferrofluid droplets, Phys. Fluids 23 (7) (2011), 072008.
[28] S.H. Tan, N.-T. Nguyen, Generation and manipulation of monodispersed ferrofluid emulsions: the effect of a uniform magnetic field in flow-focusing and T-junction configurations, Phys. Rev. E 84 (3) (2011), 036317.
[29] S.S. Leung, et al., Heat transfer in well-characterised Taylor flow, Chem. Eng. Sci. 65 (24) (2010) 6379–6388.
[30] Y. Muzychka, E. Walsh, P. Walsh, Heat transfer enhancement using laminar gas-liquid segmented plug flows, J. Heat Transf. 133 (4) (2011).
[31] R.K. Shah, S. Khandekar, On-demand augmentation in heat transfer of Taylor bubble flows using ferrofluids, Appl. Therm. Eng. 205 (2022), 118058.
[32] S.S. Leung, et al., Effect of flow characteristics on Taylor flow heat transfer, Ind. Eng. Chem. Res. 51 (4) (2012) 2010–2020.
[33] Y. Muzychka, M. Yovanovich, Laminar forced convection heat transfer in the combined entry region of non-circular ducts, J. Heat Transf. 126 (1) (2004) 54–61.
[34] P.A. Walsh, E.J. Walsh, Y.S. Muzychka, Heat transfer model for gas–liquid slug flows under constant flux, Int. J. Heat Mass Transf. 53 (2010) 3193–3201.
[35] M.T. Kreutzer, et al., Inertial and interfacial effects on pressure drop of Taylor flow in capillaries, AICHE J. 51 (9) (2005) 2428–2440.
[36] J.W. Cahn, J.E. Hilliard, Free energy of a nonuniform system. I. Interfacial free energy, J. Chem. Phys. 28 (2) (1958) 258–267.
[37] J.W. Cahn, J.E. Hilliard, Free energy of a nonuniform system. III. Nucleation in a two-component incompressible fluid, J. Chem. Phys. 31 (3) (1959) 688–699.
[38] T. Thulasidas, M. Abraham, R. Cerro, Bubble-train flow in capillaries of circular and square cross section, Chem. Eng. Sci. 50 (2) (1995) 183–199.

[39] S. Santra, S. Mandal, S. Chakraborty, Phase-field modeling of multicomponent and multiphase flows in microfluidic systems: a review, Int. J. Num. Methods Heat & Fluid Flow 10 (2020) 3089–3131.
[40] D. Lakehal, G. Larrignon, C. Narayanan, Computational heat transfer and two-phase flow topology in miniature tubes, Microfluid. Nanofluid. 4 (4) (2008) 261.
[41] F. Bai, et al., Three dimensional phase-field investigation of droplet formation in microfluidic flow focusing devices with experimental validation, Int. J. Multiphase Flow 93 (2017) 130–141.